Keratin-chitosan microcapsules via membrane emulsification and interfacial complexation

Amy Wilson,[†] Ekanem E Ekanem,[‡] Davide Mattia,[‡] Karen J Edler,*[†] Janet L Scott[†]*

[†]Department of Chemistry, University of Bath, Claverton Down, Bath, BA2 7AY, United Kingdom

[‡]Department of Chemical Engineering and Centre for Advanced Separations Engineering, University of Bath, Claverton Down, Bath, BA2 7AY, United Kingdom

* Corresponding Authors:

D.Mattia@bath.ac.uk (D. Mattia)

K.Edler@bath.ac.uk (K.J. Edler)

ABSTRACT: The continuous fabrication via membrane emulsification of stable microcapsules using renewable, biodegradable biopolymer wall materials keratin and chitosan is reported here for the first time. Microcapsule formation was based on opposite charge interactions between keratin and chitosan, which formed polyelectrolyte complexes when solutions were mixed at pH 5.5. Interfacial complexation was induced by transfer of keratin-stabilized primary emulsion droplets to chitosan solution, where the deposition of chitosan around droplets formed a core-shell

structure. Capsule formation was demonstrated both in batch and continuous systems, with the latter showing a productivity up to 4.5 million capsules per minute. Keratin-chitosan microcapsules (in the 30- 120 μm range) released less encapsulated Nile red than the keratin-only emulsion, whereas microcapsules crosslinked with glutaraldehyde were stable for at least 6 months, and a greater amount of crosslinker was associated with enhanced dye release under the application of force due to increased shell brittleness. In light of recent bans involving microplastics in cosmetics, applications may be found in skin-pH formulas for the protection of oils or oil-soluble compounds, with a possible mechanical rupture release mechanism (e.g. rubbing on skin).

KEYWORDS: Microencapsulation; membrane emulsification; keratin; chitosan; biopolymer; coacervation; layer-by-layer; polyelectrolyte complex

INTRODUCTION:

Microencapsulated oils have a wide variety of applications across a range of industries, including food,household,[1] cosmetic,[2] and pharmaceutical[3] products. Encapsulation within a polymeric shell not only allows their dispersal in a polar environment, but also offers benefits such as protection from oxygen degradation,[4] improved retention of volatile components,[1] and controlled release of the contents.[3] The diameter of microcapsules can range between 1 micrometer to a few mm,[5] making them small enough to pass through wastewater treatment plants into aquatic environments,[6] contributing to microplastic pollution when synthetic, non-biodegradable wall materials are used (e.g. PEG,[7] PMMA,[8] or melamine-formaldehyde[1]). The environment is polluted with 36,000 tons of microplastics each year in the EU alone;[9] and concerns over the implications

for aquatic life and human health have grown with the emergence of studies confirming the presence of microplastics in the entire human food supply chain.[10]

While steps have been made to tackle microplastic pollution, including enacted and proposed limited bans on plastic microbeads,[9] there remains a need to develop microcapsules based on biodegradable and non-toxic materials. Research on the use of biopolymers for microencapsulation is robust, with most investigated biopolymers including alginate, casein, whey proteins, chitosan, soy proteins, gluten, silk fibroin, zein, starch and cellulose.[11]

Oppositely charged biopolymers can form complexes with each other via attractive electrostatic forces,[12] and this mechanism is utilized in coacervation-based microencapsulation techniques such as complex coacervation[13] and layer-by-layer methods.[2]

As well as being non-toxic, renewable and biodegradable, the wall materials used for microencapsulation should be inexpensive and abundant, ideally existing in underutilized industrial waste streams. Keratin, a structural animal protein, meets all of the above requirements, with millions of tons of unutilized keratinous waste produced each year.[14] Keratin can be solubilized from waste wool or feathers by sulfitolysis, reduction or other methods,[15] is negatively charged over a range of pH values,[16] and has surface-active and emulsifying properties.[17] Keratin has been used as a building block in the synthesis of multilayer films of alternating anionic keratin and a cationic polyelectrolyte,[16] however, no examples were found in the literature of keratin being used in coacervation or layer-by-layer style microencapsulation of a liquid core.

Chitosan is the second most abundant biopolymer on the planet after cellulose, obtained from crustacean waste by deacetylation of chitin,[18] most of which has no downstream use,[19] making it another ideal sustainable biomaterial. Critically, chitosan is positively charged below its pKa (~6.5)[20] and, therefore, complexation with keratin via electrostatic interactions is likely. Chitosan

and keratin have been previously combined to prepare composite films,[21] and chitosan has been used in conjunction with other anionic biopolymers in similar microencapsulation systems.[13, 22]

Most instances of coacervate-based microcapsules in the literature use homogenization as the method of primary emulsification, however the utilization of membrane emulsification (ME) can offer several advantages.[23] In ME, the disperse phase is injected through a porous membrane into the continuous phase where droplet detachment is driven by shear stress across the membrane surface. The size of the droplets can be tuned by careful control of the process parameters, resulting in the production of monodisperse emulsions.[24] Due to the low energy of membrane emulsification however, the kinetics of adsorption of an emulsifier at the emerging oil-water (O/W) interface is critical for the production of stable emulsions with narrow droplet size distributions.[25] While soluble keratin has been reported to produce stable emulsions by ultrasonication,[17] the use of keratin in ME has not previously been attempted to the authors' knowledge.

In the present study the formation of stable microcapsules based on the electrostatic interactions between keratin and chitosan is reported for the first time. ME was utilized to generate the primary emulsion, in both batch and continuous configurations. Subsequently, the production of microcapsules from the primary emulsion was obtained by adsorption of chitosan to oppositely charged keratin at the droplet surface and crosslinking with glutaraldehyde. The properties and characteristics of the microcapsules and shell were examined by microscopy, zeta potential, and stability. Release studies were then carried out to assess the effect of chitosan absorption and cross-linking in the shell on the release of an oil-soluble dye from the encapsulated oil phase.

EXPERIMENTAL SECTION

Materials. Clean sheep's wool was obtained from Wingham Wool Work. Sunflower oil was obtained from Tesco and used as the disperse phase (DP) for the primary emulsion. Urea ≥98%, sodium metabisulfite ≥99%, tris(hydromethyl)aminomethane ≥99.8%, sodium dodecyl sulfate (SDS) ≥95%, Hydrochloric acid (HCl, 35%) and sodium hydroxide (NaOH, 98%) were purchased from Fisher Scientific, UK. HCl and NaOH were diluted to 0.1M as stock solution for pH adjustments; low molecular weight chitosan, acetic acid ≥99%, fluorescein isothiocyanate (FITC) ≥90%, methanol ≥99.9%, Nile red ≥98%, hydrochloric acid 32% and glutaraldehyde (GTA) solution grade II 25 wt% in H_2O were obtained from Sigma Aldrich UK and used without further purification.

Preparation of biopolymer solutions. Keratin was extracted from wool by using sodium metabisulfite as a reducing agent to cleave disulfide bonds.[15] Clean sheep's wool (30 g) was heated in 1 L deionized water containing 8 M urea, 0.5 M sodium metabisulfite, 0.2 M tris base and 0.2 M SDS (pH 7, adjusted using NaOH) at 65 °C for 5 h. The resulting aqueous extract was passed through a 50 μm mesh sieve and dialyzed against deionized water for 6 days using a cellulose tube membrane (MWCO 8 kDa), replacing the water daily. The solution was then diluted to 1 wt% concentration with deionized water, where the initial concentration of keratin was determined by loss on drying method. For the loss on drying method, approximately 5 g of sample were dried at 50 °C until no further change in mass was noted, and the mass of residual solids was calculated as a percentage of the initial sample mass.

Chitosan (1 wt%) was solubilized in 1 wt% acetic acid by overnight stirring at room temperature. The solution was vacuum filtered (Whatman, Grade 1), diluted to the desired concentration with deionized water and adjusted to pH 5.5 using NaOH.

Zeta potential of keratin solution. The prepared keratin solution, to be used as the continuous phase (CP) of the primary emulsion, was adjusted to pH values between 2-12 using NaOH and HCl. Each sample was loaded into a folded capillary cell and the zeta potential was measured using a Zetasizer Nano ZSP instrument (Malvern Instruments, Malvern, UK). Two samples were prepared for each pH value, each measured in triplicate.

Turbidity measurement. Mixtures of keratin and chitosan solutions were prepared with a final concentration of 0.3 wt% chitosan and a range of keratin concentrations (0, 0.01, 0.05, 0.1, 0.2, 0.3 or 0.5 wt%). After stirring for 20 min at room temperature, the samples were diluted 10x with deionized water and the transmission at 300 nm was measured using a Jenway UV-vis spectrophotometer (Cole-Palmer, St Neots, UK). Turbidity was calculated by subtraction of %Trans from 100.

Viscosity measurement. The viscosity of the 1 wt% keratin solution and sunflower oil was measured using a Discovery HR-3 rheometer (TA Instruments, New Castle, USA). A shear rate sweep was conducted at 25 °C from 0.1 to 1000 1/s using a 40 mm cone (angle = 1deg:0min:25 sec) and plate (gap = 29 μm).

Interfacial tension measurement. The interfacial tension between the 1 wt% keratin solution and sunflower oil at 25 °C was measured using a FTA1000 B Class tensiometer (First Ten Angstroms, Portsmouth, USA) by the rising drop method. The sunflower oil disperse phase was extruded from a hooked needle into the 1 wt% keratin continuous phase and the surface tension was determined from the shape of the rising drop before droplet detachment. An average of 3 measurements was taken (drop volume ~4 μL).

Stirred cell membrane emulsification (SCME). O/W emulsions were prepared by SCME using a Liquid Dispersion Cell (Micropore Technologies) and ringed, stainless steel, disc

membranes. Prior to use in membrane emulsification, the stainless-steel membranes (both disc and tubular) and additional inner rod underwent a standard cleaning procedure.[26] Briefly, the items were immersed sequentially in an ultrasonic bath for 1 minute in deionized water, 4 M NaOH, deionized water, 10 % wt citric acid, and finally deionized water. The items were soaked for 10 minutes in the acid and base solutions after sonication and were rinsed with tap water afterwards, before transfer to deionized water.

Sunflower oil (10 mL) was introduced by syringe pump through the pores of the membrane into the cell containing 90 mL keratin solution, where droplet detachment was facilitated by the wall shear generated from the paddle stirrer.

Using DoE software (MODDE Pro 12.1), a fractional experimental design with a linear model was implemented to explore the size and span (as responses) of emulsions generated using the dispersion cell. Three controllable emulsification parameters (pore size, stirring speed and injection rate) were investigated as factors. The diameter of the pores were either 10 or 30 μm, while the stirring speed and injection rate ranged from 400 to 1100 rpm and 0.3 to 0.5 mL/min respectively. 12 experiments were conducted including 4 center points (3 repeats).

Cross flow membrane emulsification (xME). A bespoke system was designed and commissioned, consisting of a stainless-steel (SS) tubular membrane and its assembly in the membrane housing (Figure 1).

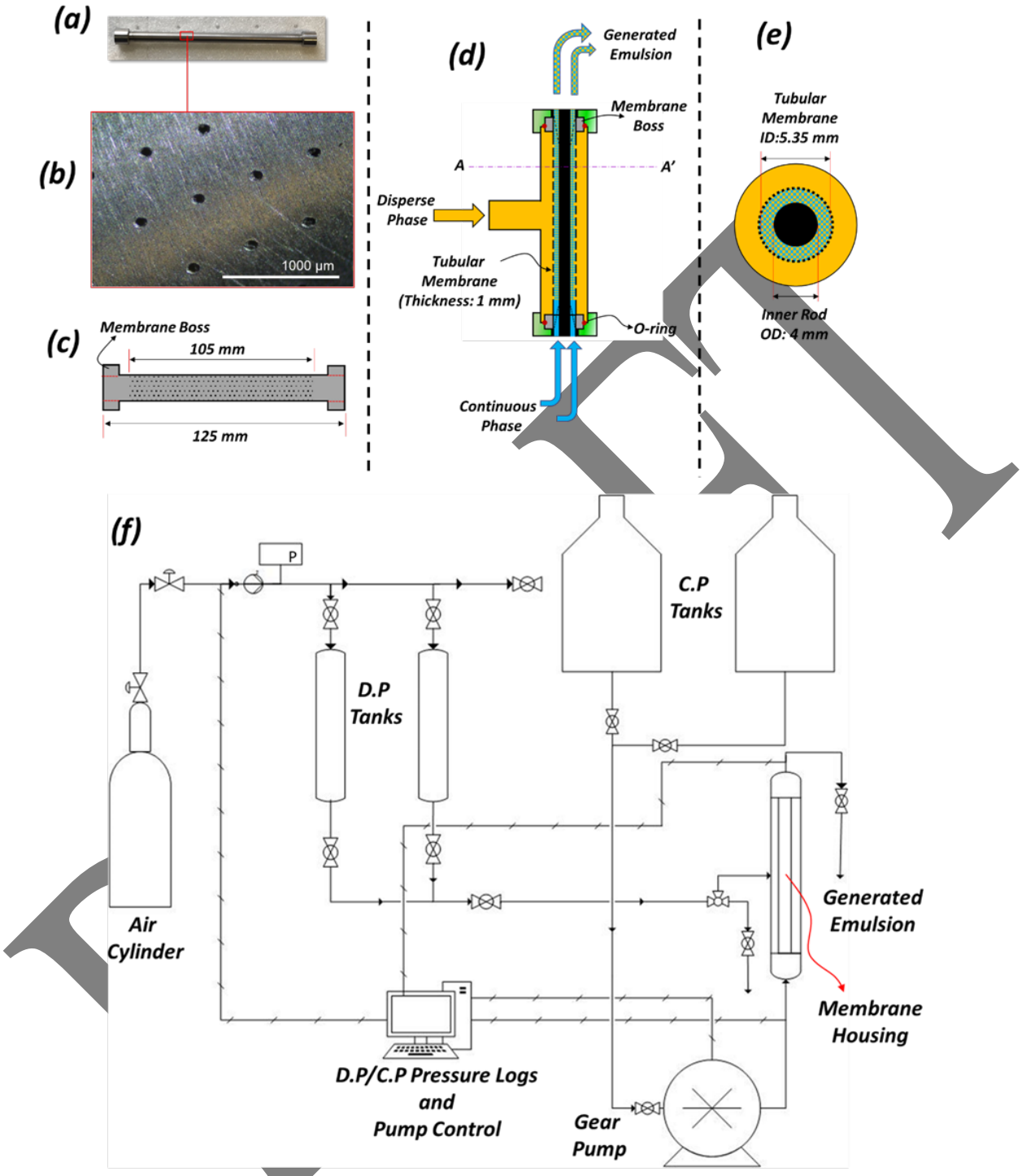

Figure 1: Stainless-Steel Tubular membrane and assembly in membrane housing (a) Tubular membrane; (b) Optical micrograph of tubular membrane pores; (c) Schematic showing tubular membrane, its dimensions and boss positions; (d) Schematic showing tubular membrane assembly

in membrane housing; (e) Schematic showing cross-section of A-A' on membrane assembly; (f) Process flow diagram for the continuous cross-flow membrane emulsification apparatus used.

The stainless-steel tubular membrane and inner rod were obtained from Microkerf, Leicester, UK. The membrane (Figure 1a-c) was fabricated from a stainless tube with ID 5.35mm and 30 μm pores (Figure 1b) laser drilled to cover the middle 105 mm of its 125 mm length with a 500 μm pitch.

The stainless-steel tubular membrane was cleaned as described for the disc membrane before assembly in the membrane housing (Atech Innovations, Germany). For assembly into the housing (Figure 1d), the inner rod 4 mm OD was inserted into the SS membrane's lumen and held into place by supports with drilled slits to allow for the cross flow of the CP within the created annulus (Figure 1d) bounded by the inner wall of the SS membrane and outer wall of the inner rod (4 mm). The membrane housing (and assembled components) was then attached to the continuous crossflow membrane emulsification rig (Figure 1f). The CP and DP were pumped to the SS membrane housing at predetermined flowrates (via gear pump) and pressures (via compressed air), respectively, for crossflow droplet generation. The DP pressures, CP flowrates and resultant transmembrane pressures (TMP) for each droplet generation sample were acquired and logged using LabVIEW (National Instruments).

Microcapsule preparation. Primary emulsion droplets were isolated from the keratin solution by gravitational creaming in the absence of coalescence and 1 mL creamed droplets were mixed with 1 mL deionized water and immediately added to 10 mL 0.25 wt% chitosan. This was followed by the addition of 0, 25 or 50 µL GTA solution under stirring at room temperature. Samples were placed on a roller for 1 h and subsequently stored at room temperature.

Imaging and sizing of emulsion and microcapsules. Optical micrographs were captured using a SP400 microscope and digital camera (Olympus). Volume-weighted particle size distributions were obtained using a Mastersizer 3000 particle size analyzer and wet dispersion unit (Malvern Instruments) operating at 2000 rpm. The D_{50} and span were recorded.

Monitoring of adsorption of chitosan. The zeta potential of primary emulsion droplets was measured before and after addition of the creamed droplets to chitosan solutions of different concentrations (0.001, 0.005, 0.01, 0.05, 0.1, 0.5, or 1 wt %) to monitor the adsorption of chitosan at the droplet surface. A washing step with deionized water was included before and after stirring in chitosan solution to remove excess polyelectrolyte. The zeta potential was measured as described for the keratin solution.

Fluorescence microscopy. Fluorescently-labelled chitosan was prepared by addition of 100 mg FITC in 100 mL methanol to 100 mL 1 wt% chitosan solution and stirred overnight in the dark at room temperature.[27] The chitosan was precipitated with NaOH and unreacted FITC was removed by centrifugation (8000 x g, 10 min). The precipitate was washed with deionized water until the supernatant showed no fluorescence. The FITC-labelled chitosan was dissolved in 1 wt% acetic acid solution and dialyzed against deionized water for 3 days in the dark, replacing the water daily. The concentration of chitosan in the final solution was determined by loss on drying method and the solution was diluted with deionized water to 0.25 wt%. The pH was adjusted to 5.5 using NaOH.

Fluorescence micrographs were captured using an EVOS M5000 Imaging System (Thermo Fisher Scientific) fitted with a green fluorescent protein (GFP) light cube with excitation (λ_{ex}) and emission wavelengths (λ_{em}) of 470 nm and 525 nm respectively for the visualization of FITC-labelled chitosan, and a red fluorescent protein (RFP) light cube (λ_{ex} = 531 nm, λ_{em} = 595 nm) for

visualization of the Nile red stained oil respectively. Prior to imaging, the microcapsules were dispersed in deionized water to reduce background fluorescence from unadsorbed chitosan.

Release of encapsulated Nile red. Both un-crosslinked and crosslinked microcapsules were prepared using sunflower oil stained with Nile red (1 mg/mL) to make the primary emulsion. As a control, primary emulsion controls were prepared by mixing 1 ml creamed droplets with 1 mL deionized water and addition to 10 mL 1 wt % keratin solution to ensure the same degree of dilution of the primary emulsion droplet suspension in all samples. Unstained sunflower oil (5 mL) was gently placed on top of each sample using an automatic pipette. The samples were either left static at room temperature for 5 days, or centrifuged immediately (15 m, 5000 x g). An aliquot (1 mL) was taken from the center of the oil layer and the absorbance was measured at 520 nm by UV-Vis spectrophotometry. An average result was taken from three repeats. A standard curve was prepared by measurement of known concentrations of Nile red stained sunflower oil, diluted with unstained oil.

RESULTS AND DISCUSSION

Complexation between keratin and chitosan. The zeta potential of the extracted keratin between pH 2-12 was negative, with the magnitude of the net surface charge increasing with alkalinity (Figure 2) due to deprotonation of its amino groups. The values reported here are more negative than reported in the literature,[16, 28] attributed to the use of the anionic surfactant SDS in the extraction process, included to prevent the major aggregation of solubilized keratin during dialysis. Previous research on the use of SDS in the extraction of feather keratin suggests that while most of the SDS was removed by dialysis, some remained complexed to keratin molecules which would impart a more negative overall charge.[29]

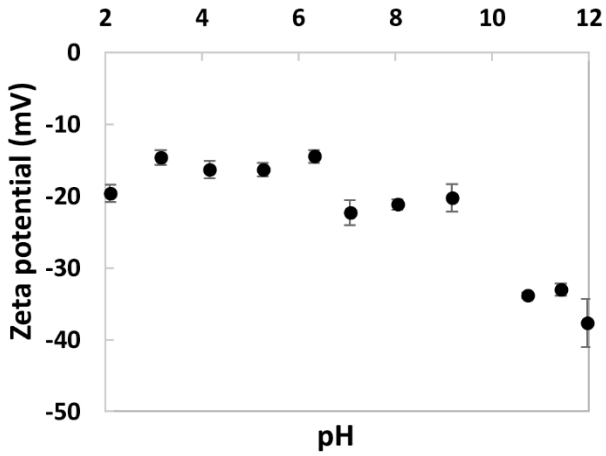

Figure 2. Zeta potential of keratin solution as a function of pH. Error bars represent standard deviation from 3 measurements.

Since the keratin was negatively charged, it was expected to interact with chitosan to form polyelectrolyte complexes by opposite charge interactions at an appropriate pH below chitosan's pKa (~6.5).[30] Since the magnitude of the charge on the keratin decreased with increasing acidity, pH 5.5 was selected to ensure both polyelectrolytes carried a moderate charge.

An opaque dispersion was observed when solutions of keratin and chitosan solution were mixed together at pH 5.5, indicating formation of insoluble particles. The opacity of the dispersion became more pronounced with increased keratin content (Figure 3a).

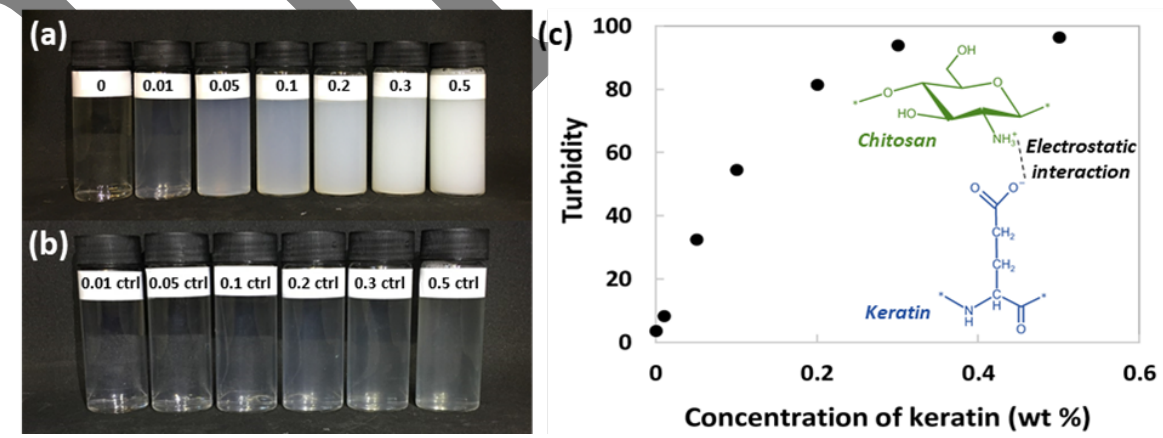

Figure 3. (a) Dispersions of mixed chitosan and keratin solutions (0.3 wt% chitosan, 0-0.5 wt% keratin, pH 5.5); (b) controls containing only keratin solution (0-0.5 wt% keratin, pH 5.5); (c) turbidity of dispersions containing 0.3 wt % chitosan and 0-0.5 wt % keratin, pH 5.5, diluted 10x with deionized water. Error bars (mostly smaller than the dot size) represent the standard deviation from 3 measurements. The diagram shows the proposed interaction mechanism of keratin and chitosan.

The degree of opacity was measured by turbidity quantification (Figure 3c). There was an initial rapid rise in turbidity with increasing keratin content due to the increased presence of light-scattering polyanion-polycation complexes, and then a levelling off at higher concentrations, which could be a result of multiple scattering effects due to a high concentration of particles, or sedimentation of larger particles causing increased transmission of light through the sample. While complex assembly is thought to be driven mainly by the long-range electrostatic attraction between keratin's negatively charged amino acid side chains and chitosan's positively charged amino groups, medium-range hydrophobic interactions and short-range hydrogen bonding can also contribute to complex formation and stability.[12] Wool keratin consists of a variety of amino acids with polar, non-polar and ionizable side chains that allow for multiple interactions to take place.[31] Both keratin and chitosan contain groups that can participate in hydrogen bonding, i.e. chitosan's hydroxyl groups and cysteine and serine in keratin, which contain a hydroxyl and sulfhydryl group respectively. Although the deacetylated chitosan used in this work is hydrophilic in nature,[32] hydrophobic interactions may take place between keratin's non-polar amino groups (e.g. leucine, valine) and chitosan's acetyl groups.

Primary emulsion generation by stirred cell membrane emulsification. After confirmation of complexation between keratin and chitosan, the next step was to apply the interaction at the interface of an emulsion. The membrane emulsification of the primary emulsion (stabilized by keratin) was explored by small batch (100 mL) SCME to scope the droplet size range and uniformity of generated emulsions prior to scaling up to continuous crossflow membrane emulsification (xME). Table S1 summarizes the DOE and experimental data for the 12 experiments conducted. Droplets with median volume diameters (D_{50}) between 30 - 126 µm (Figure 4a), were generated using a membrane pore diameter of either 10 or 30 µm and varying the injection rate and stirring speeds between 0.2 - 0.5 mL/min, and 400 - 1100 rpm, respectively. Results from the DOE showed a good fit and future prediction precision of $R^2 = 0.99$ and $Q^2 = 0.87$ for the D_{50}, (Table S2), which allowed the estimation of D_{50} at any given space within the range of parameters tested (Figure 4b). This was confirmed by validation experiments carried out with both membrane pore sizes investigated, with excellent results (Table S3).

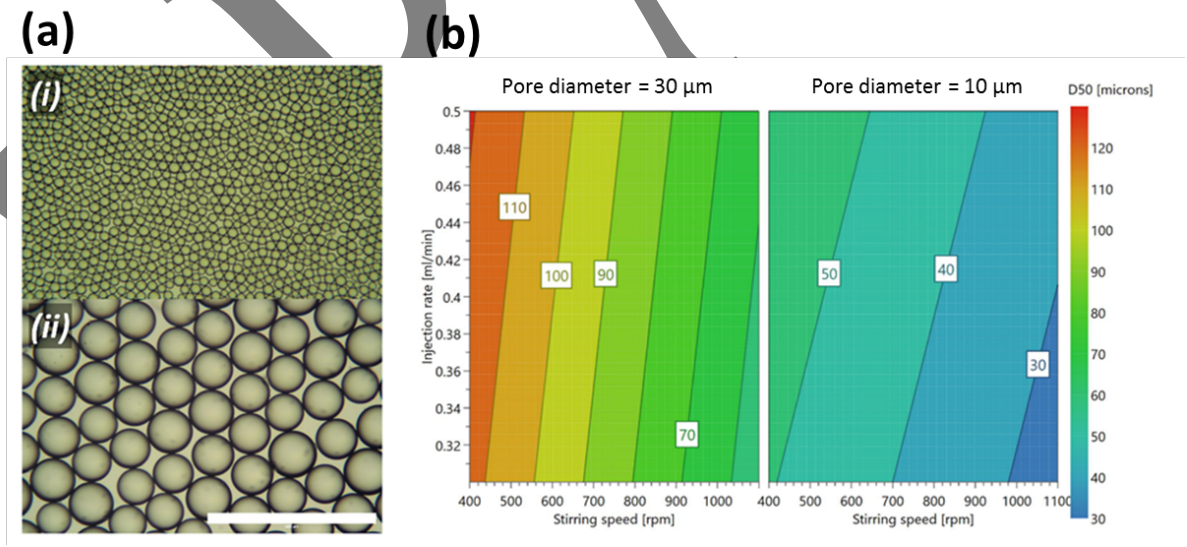

Figure 4. (a) Optical micrographs of smallest and largest keratin stabilized microdroplets produced by stirred cell membrane emulsification of sunflower oil in 1 wt % keratin solution: (i) Experiment

3: d_p = 10 μm, injection rate = 0.3 mL/min, stirring speed = 1100 rpm, D_{50}= 29.9 μm; (ii) Experiment 6: d_p = 30 μm, injection rate = 0.5 mL/min, stirring speed = 400 rpm, D_{50} = 126 μm. Scale bar = 500 μm. (b) 4-D contour plots showing the predicted D_{50} (median volume diameter) of emulsions of sunflower oil in 1 wt% keratin solution produced by stirred cell membrane emulsification.

The D_{50} was dependent on all factors included in the DOE, with pore size having the greatest influence, followed by stirring speed (Table S2). The size of the pores is a major factor in determining the size of the droplets produced by membrane emulsification, with droplets produced here being 2-6 times larger than the pore diameter, in agreement with the 2-10 ratio found in the literature.[33] The stirring speed had a strong influence on droplet diameter as it generated the shear which causes droplet detachment.[34] Stirring speeds between 400-1100 rpm enabled the controlled access to a wider range of droplet size categories for the 30 μm pore size than the 10 μm pore size, (Figure 4b). Although a higher injection rate results in a greater volume of disperse phase permeated through the membrane before droplet detachment and, hence, in larger droplets,[34] its effect in the design space used here was minimal compared to other factors (Table S2). This result also implies the absence of any transition from dripping to jetting regimes or vice versa, which would have resulted in a clear discontinuity in droplet diameter.

The span, a dimensionless number indicating the width of the distribution of the emulsions, ranged from 0.368 to 0.923 (Table S1). The DOE was used to identify the parameters where span would be lowest, and therefore the droplets would be most uniform. The model was tuned in order to improve the fit and future prediction precision by log transformation, removal of an insignificant term (injection rate), and addition of an identified squared term (stirring speed), resulting in an R^2

value of 0.95 and Q^2 value of 0.79. For the 30 μm pore diameter, DOE results indicated that low stirring speeds promoted monodispersity. Within the design space, droplets generated at 400 rpm were, therefore, most uniform. An opposite effect was observed with the 10 μm membrane whose uniformity increased slightly with increasing stirring speed. The impact of stirring speed was more significant when using the larger pore size, and when the stirring speed was higher. It was concluded therefore that droplet breakup at high shear was responsible for the relatively poor span seen in some samples from membranes with a larger pore size, and the lower predictability of the span model versus the D_{50} model, and hence the minor upper limit deviation of 3.0 % and 3.5 % for the 10 μm and 30 μm pore membranes respectively in span validation experiments (Table S3).

Scale-up with crossflow membrane emulsification. Using as a starting point the conditions which gave the lowest span in the stirred cell setup (experiment 6, D_{50} of 126 μm, span = 0.368, with a 30 μm pore membrane), the wall shear (τ_{SMCE}) of 2.043 Pa was approximated using eq S3-S6 for the xME equipment design values of Impeller diameter (D) = 0.03 m, Tank diameter (T) = 0.035 m, blade height (b) = 0.011 m, number of blades (n_b) = 2; membrane morphology values of r_1 and r_2 of 0.008 mm and 0.011 mm as the respective outer and inner radii of the porous region of the ringed membrane; CP properties μ_c and ρ_c of 0.00101 Pa.s and 1000kg/m^3, respectively; and emulsification ω of ≈ 41.9 s^{-1} @ 400 rpm.

This resulted in significantly larger droplets, with D_{50} = 199 μm and a span = 0.708, for approximate DP Weber number (We_d) of 4.1 x 10^{-4} and CP capillary number (Ca_c) of 0.171, respectively (Figure 5 (i)), evaluated by eq S1 and S2. As the membrane in the xME configuration has approximately 10x more pores than the SCME disc membrane owing to the increased pore area of the membrane, a proportionally higher DP flowrate was needed to maintain the same We_d (~5 mL/min of sunflower oil in the xME system compared to 0.5 mL/min in the SCME). The CP

flowrate needed to obtain similar shear, approximated by equation S7, was applied to the xME (i.e 300 ml/min).

From this first value, the xME system was further tuned following three (3) strategies (Figure 5a): increasing Ca_c at constant We_d; reducing We_d at constant Ca_c; and a combination of increasing Ca_c and reducing We_d.

For the first strategy, droplet diameters with D_{50} approaching the values in the SCME were obtained by increasing the shear of the xME system to Ca_c values of ≈ 0.393 (700 ml/min) from 0.171 at nearly constant We_d (Figure 5a path A) which resulted in droplets generated with a D_{50} of 123 μm but with a higher span of 0.892 (Figure 5-ii) and ~4x higher droplet throughout. The higher span and broadening of the droplet size distribution (cfr. Figure 5-ii) of a narrowing jetting regime is characterized by jet breakup at multiple points of the dispersed phase jet.[35]

For the second strategy, the We_d was reduced ~4x to 1.1 x 10^{-4} (cfr. Figure 5a path B) at constant Ca_c (0.171), leading to an increased diffusion of keratin from the bulk CP to the interface and, consequently, promoting droplet stability due to a slower dispersed phase droplet growth. However, further We_d reduction to 4.3 x 10^{-5} (Figure 5 path C) resulted in droplets with a D_{50} reduction from 167 μm to 160 μm but an increased span from 0.559 to 0.624. Continuous We_d reduction from 4.3 x 10^{-5} (Figure 5-iv) to 1.2 x 10^{-5} (Figure 5-v) resulted in progressively smaller yet less uniform droplets (Figure 5a path D). This reduced uniformity with reducing DP inertia is due to, again, an onset of thinning jetting as evident from the increased number of small droplets (Figure 5-v).

In both cases of thinning jetting (i.e. Figure 5-ii,v), larger droplets were observed in the extreme of point (ii) as a result of poor keratin interface saturation of small microdroplets formed at the inception of jetting, with a large surface area that are not properly coated with keratin which

coalescence to form the larger droplets. This occurred less in point (v) due to lower We_d (hence, lower droplet generation frequencies) that enabled interface saturation at the inception of jetting. The formation of large droplets at high shear are seldom observed in surfactant systems due to the smaller molecular size of surfactants which promotes fast migration to the interface.[35]

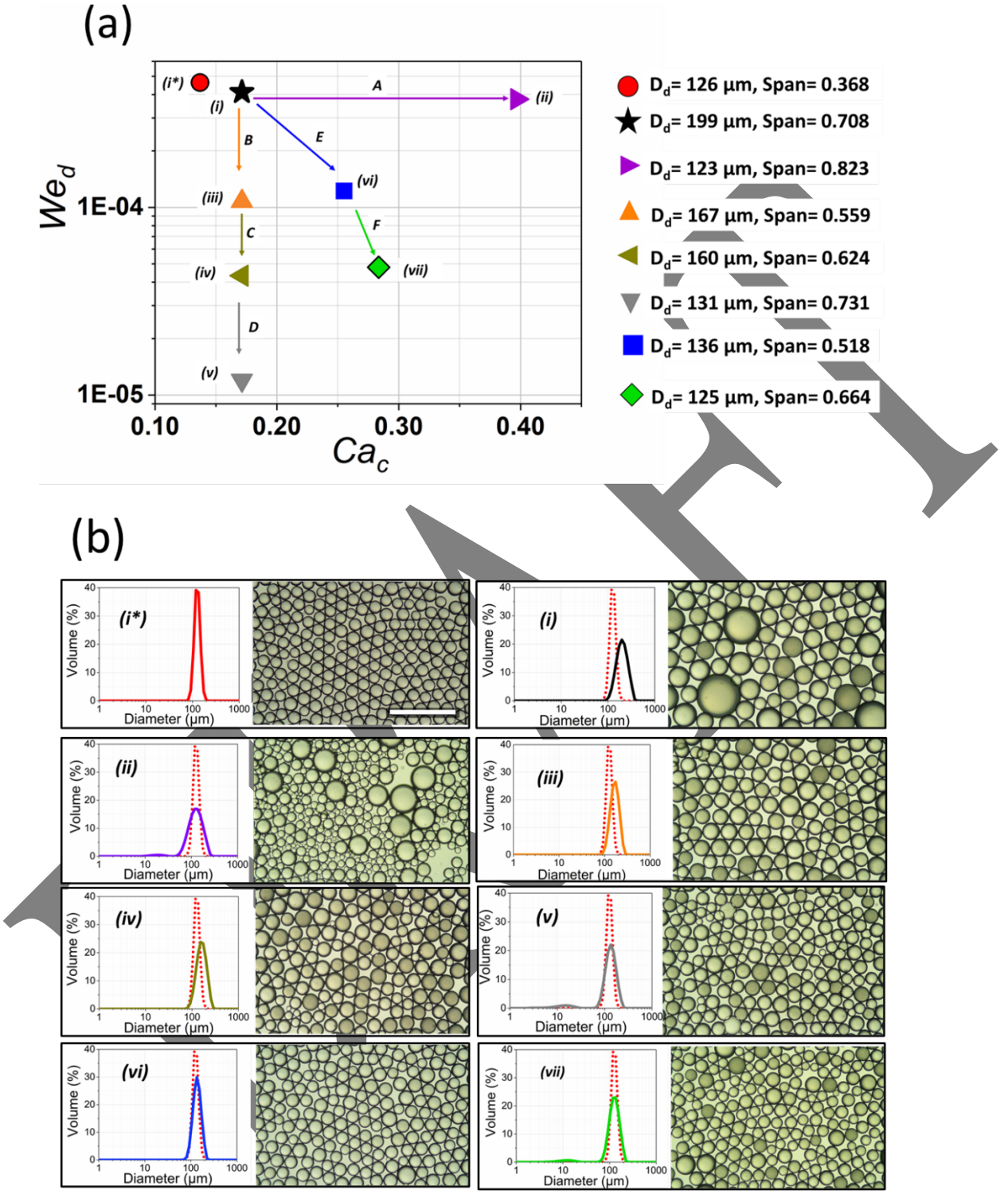

Figure 5. (a) We_d-Ca_c plot showing keratin stabilized microdroplets produced using the SCME and crossflow membrane emulsification rig. For XME, Path A shows Ca_c increase, Paths B,C and

D show We_d reduction, while Paths E and F show simultaneous increase in Cac and reduction in We_d; (b) Size distributions and optical micrographs of keratin stabilized microdroplets produced using (i*) SCME (Experiment 6: D_{50} = 126 μm, Span= 0.368) and (i)-(viii) xME; insets show particle size distributions, using i* as a reference in all distributions. For (a) and (b), (i) D_d = 199 μm, Span= 0.708; (ii) D_d = 123 μm, Span= 0.823; D_d = 167 μm, Span= 0.559; D_d = 160 μm, Span= 0.624; D_d = 131 μm, Span= 0.731; D_d = 136 μm, Span= 0.518; D_d = 125 μm, Span= 0.664.

Paths A, B, C and D demonstrate droplet generation scenarios where increased Ca_c to We_d ratios were implemented to obtain droplets with $D_{50} \approx D_{50,SCME}$. For the third strategy, an increased Ca_c to We_d ratio was accomplished by a simultaneous increase in Ca_c and decrease in We_d (i.e. Figure 5 paths E and F). This was done just enough to reduce droplet size to avoid thinning jetting. Point (vi) of Figure 5 depicts droplets formed at a Ca_c of 0.256 (450 mL/min) and We_d of 1.2 x 10^{-04} to obtain droplets with a D_{50} of 136 μm and span of 0.518 (Figure 5-vi) that were more uniform than points (i) and (ii). Further simultaneous Ca_c increase with We_d reduction led to droplets possessing a D_{50} of 125 μm and span of 0.664 (Figure 5-vii). This was carried out at a Ca_c of 0.280 (500 mL/min) and We_d of 4.8 x 10^{-05} (Figure 5-vii).

This investigation, therefore, showed how the operational space of We_d-Ca_c can be leveraged to strategically tune the properties of generated emulsions with the xME.

Microcapsule formation and stability. Zeta potential measurements were used to monitor the deposition of chitosan at the surface of keratin-stabilized emulsion droplets to form the microcapsule shell. The untreated primary emulsion droplets had a negative zeta potential (between -20 to -30 mV) due to the negatively charged keratin at the interface (Figure 6a). After

treatment with chitosan, charge reversal occurred, indicating the adsorption of positively charged chitosan at the droplet surface with the zeta potential increasing sharply with increasing concentration of chitosan and then levelling off at 20-30 mV, suggesting adsorption saturation. As such, a concentration of 0.25 wt% chitosan was chosen as the optimal value.

The microcapsule structure was visualized by fluorescence microscopy of samples made with FITC-labelled chitosan and Nile red-stained sunflower oil. The location of FITC-chitosan, after removal of excess from the continuous phase by dilution in water, was concentrated at the droplet surface (Figure 6b-i), and the location of the oil phase was confirmed inside the microcapsules (Figure 6b-ii). Both images merged together (Figure 6b-iii) demonstrate a core-shell structure, confirming the Zeta potential results.

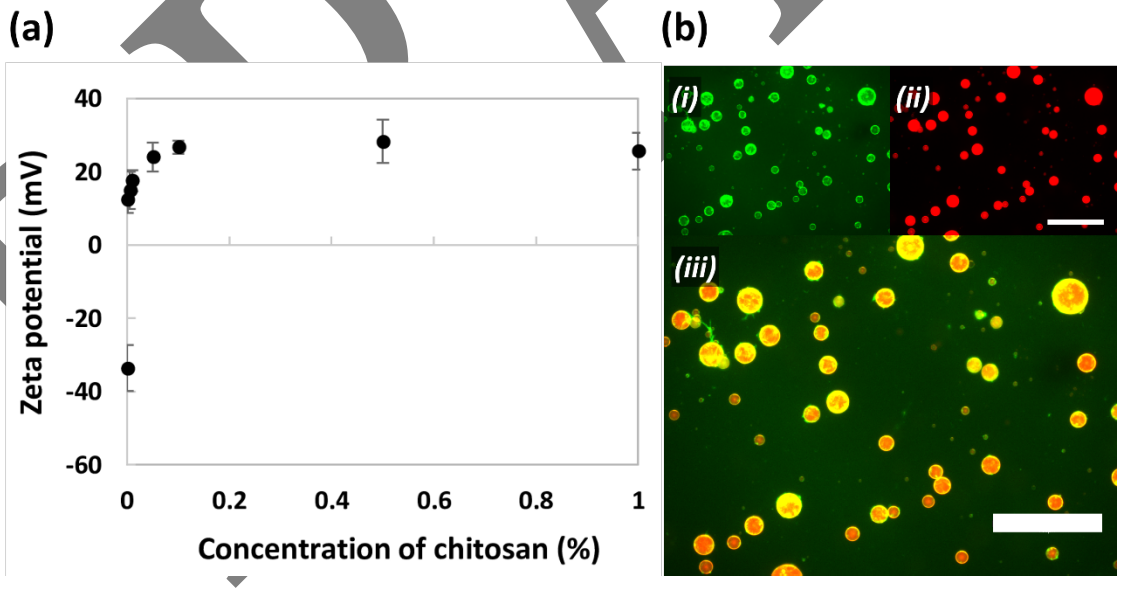

Figure 6. (a) Zeta potential of keratin-stabilized oil droplets after treatment with 0-1 wt % chitosan solution. Error bars represent standard deviation from 3 measurements. (b) Fluorescence

microscopy images of keratin-chitosan microcapsules containing sunflower oil. (i) FITC-labelled chitosan (λ_{ex} = 470 nm, λ_{em} = 525 nm); (ii) Nile red stained sunflower oil (λ_{ex} = 531 nm, λ_{em} = 595 nm); (iii) merged. Scale bars = 750 μm.

The attraction between biopolymers within a polyelectrolyte complex differs in strength depending on the characteristics of the biopolymers in question and the environmental conditions,[12] and coacervate microcapsules sometimes require chemical crosslinking to give strength and stability to the shell.[36] Therefore, different quantities of glutaraldehyde solution were added during microcapsule formation to crosslink between the amino groups of keratin and chitosan molecules.

The stability of the crosslinked and un-crosslinked microcapsules was assessed in terms of both size and integrity. For the former, storage for 6 months resulted in no significant change to the size distribution or D_{50} of the crosslinked microcapsules (Figure 7a-ii,iii, Figure S1), whereas a significant increase in average particle size was observed in the un-crosslinked sample (Figure 7a-i), suggesting that crosslinking enhances long-term stability. GTA addition increased the initial D_{50} due to crosslinking of microcapsules into clusters, which the laser cannot distinguish from a single particle, hence the greater variability in results for the most highly crosslinked sample containing 50 μL GTA solution.

The stability of the microcapsules was further investigated by studying the release of an encapsulated dye from the microcapsules into an external free oil phase under both static and dynamic conditions. After 5 days of static incubation at room temperature, significantly less Nile red was released from the microcapsules as compared with the primary emulsion (Figure 7b),

probably due to a gel-like coacervate network at the interface, which is thought to reduce permeability to small molecules.[37] Upon applying centrifugal force, while all microcapsule samples released less dye than the primary emulsion, the percentage Nile red release from microcapsules crosslinked with 50 μL GTA was around 10 times higher than un-crosslinked microcapsules or those crosslinked with 25 μL GTA. This was attributed to a more rigid, brittle shell caused by a high number of covalent crosslinks between biopolymer molecules,[38] making the most highly crosslinked capsules more susceptible to breakage under the application of force. The observation of non-spherical microcapsules only in samples treated with GTA (Figure 7a arrows) supports the view of reduced elasticity and fluidity of the interfacial membrane as a result of crosslinking. These characteristics could be tailored by changing the crosslinker, e.g. using genipin, a plant sourced crosslinking agent.[39]

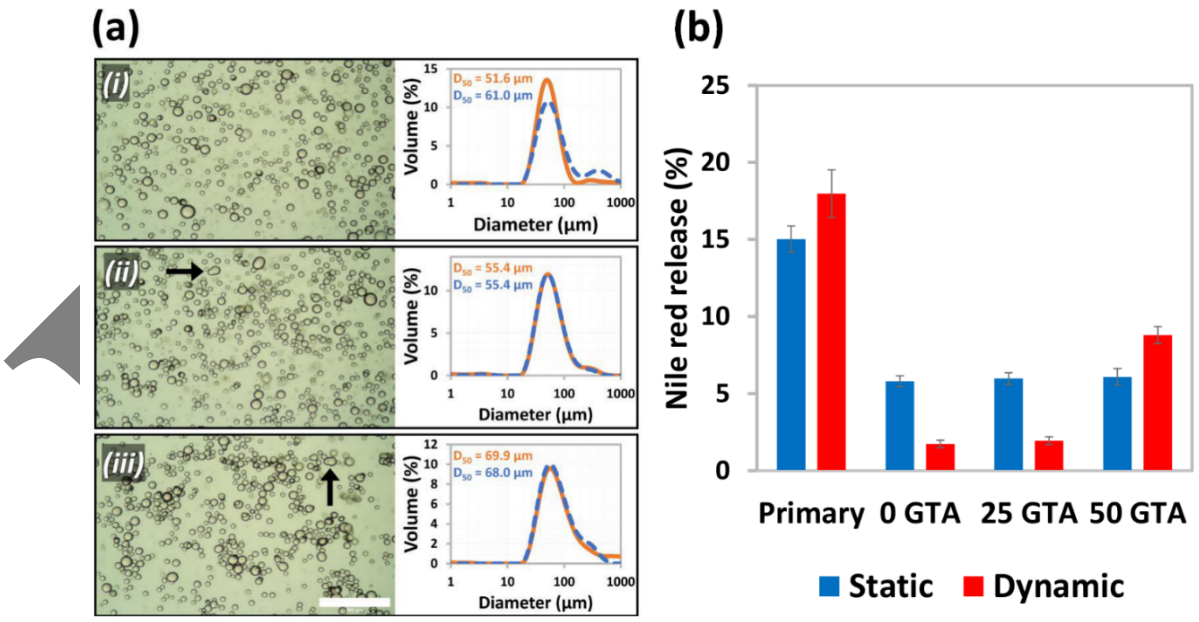

Figure 7. (a) Optical micrographs and particle size distributions of keratin-chitosan microcapsules: (i) un-crosslinked (ii) crosslinked by addition of 25 μL glutaraldehyde solution per 10 mL sample; (iii) crosslinked by addition of 50 μL glutaraldehyde solution per 10 mL sample, immediately after

synthesis (orange solid line) and after 6 months of ambient storage (blue dashed line). Scale bar = 500 μm. Arrows point to irregular structures. (b) Percentage release of Nile red from primary emulsion droplets stabilized by keratin alone vs keratin-chitosan microcapsules crosslinked with 0-50 μL glutaraldehyde solution per 10 mL sample, after 5 days static incubation at room temperature, or 15 min centrifugation (5000 x g). Error bars represent standard deviation from 3 measurements.

Productivity and Scale-up. The concentration and frequency of generated emulsions are important indices in determining the ideal emulsification conditions for scale-up. In the continuous xME, the generation of smaller droplets requires high CP flowrates, which results in a less concentrated emulsion. The use of an inner rod alleviates this problem,[40] with a 79% increase in droplet concentration compared to the case without a rod in the present work. To obtain the same droplet concentration in a system without the inner rod, recirculation of the CP would be required to meet the high shear requirement, resulting in a multiple-pass system, with negative effects on emulsion quality and energy consumption.[6, 41]

Scale up with the continuous xME also showed increased droplet generation frequency, as compared to the batch SCME, leveraging an increased membrane surface area. Consequently, a higher DP flux and emulsion productivity was achieved. Considering the data in Figure 4, although $D_{50} \approx D_{50,SCME}$ for point (ii), a droplet generation frequency of 76,168 droplets/s (equivalent to about 4.5 million droplets per minute) was obtained due to the xME's membrane pore area being ~10 times that of the SCME for the same DP flux. Further increases in droplet generation, while maintaining emulsion quality, can be obtained by increasing the membrane diameter and/or reducing the pitch length between pores. For example, doubling the inner diameter

of the membrane at constant annular diameter and membrane thickness, or doubling the length of the membrane would double the frequency of produced droplets produced at point (vii) conditions to ~51,000 droplets/s. Reducing the pitch length by 50% would have the greatest productivity effect by increasing the droplet generation frequency 4-fold to ~103,000 droplets/s. A combination of the 3 changes would result in a 16-fold higher droplet generation frequency. These values, together with numbering-up strategies, show that the keratin-chitosan microcapsules could be produced at industrial scale.

CONCLUSIONS

The production of stable microcapsules using renewable and biodegradable biopolymer wall materials keratin and chitosan is reported here for the first time. The compatibility and scale-up potential of the formulation was demonstrated with membrane emulsification. Turbidity measurements confirmed the complexation of keratin and chitosan at pH 5.5 which was linked to electrostatic attraction arising from their opposite charges, and chitosan was seen to adsorb at the surface of keratin-stabilized primary emulsion droplets by zeta potential measurements and fluorescence microscopy. Using ME it was possible to generate primary emulsion droplets with diameters of 30-126 μm and a span as low as 0.394.

Keratin-chitosan microcapsules crosslinked with GTA showed significant stability over time, with no increase in size after 6 months in storage under ambient conditions. Considering the non-toxicity and biocompatibility of keratin and chitosan, the stability of microcapsules at skin-pH and possible release mechanism of mechanical rupture (e.g. rubbing on skin), these capsules may find use in cosmetic, personal care or biomedical products.

ASSOCIATED CONTENT

Supporting Information

The Supporting Information includes further information on Crossflow membrane emulsification apparatus, Design of Experiments, shear stress approximations and particle stability (PDF). It is available free of charge via the Internet at http://pubs.acs.org.

Notes

The dataset supporting this paper is openly available from the University of Bath data archive at https://researchdata.bath.ac.uk/id/eprint/966.

ACKNOWLEDGMENTS

The authors would like to thank the EPSRC for funding this project (Grant EP/P027490/1).

REFERENCES

1. Bône, S.; Vautrin, C.; Barbesant, V.; Truchon, S.; Harrison, I.; Geffroy, C., Microencapsulated Fragrances in Melamine Formaldehyde Resins. *CHIMIA International Journal for Chemistry* **2011,** *65* (3), 177-181. DOI: 10.2533/chimia.2011.177.
2. Carvalho, A. G. S.; Silva, V. M.; Hubinger, M. D., Microencapsulation by spray drying of emulsified green coffee oil with two-layered membranes. *Food Research International* **2014,** *61*, 236-245. DOI: https://doi.org/10.1016/j.foodres.2013.08.012.
3. Mishra, N.; Rai, V. K.; Yadav, K. S.; Sinha, P.; Kanaujia, A.; Chanda, D.; Jakhmola, A.; Saikia, D.; Yadav, N. P., Encapsulation of Mentha Oil in Chitosan Polymer Matrix Alleviates Skin Irritation. *AAPS PharmSciTech* **2016,** *17* (2), 482-492. DOI: 10.1208/s12249-015-0378-x.
4. Huang, J.; Wang, Q.; Li, T.; Xia, N.; Xia, Q., Multilayer emulsions as a strategy for linseed oil and alpha-lipoic acid micro-encapsulation: study on preparation and in vitro characterization. *J Sci Food Agric* **2018,** *98* (9), 3513-3523. DOI: 10.1002/jsfa.8870.
5. Dragostin, I.; Dragostin, O.; Pelin, A.-M.; Grigore, C.; Lăcrămioara Zamfir, C., The importance of polymers for encapsulation process and for enhanced cellular functions. *Journal of Macromolecular Science, Part A* **2017,** *54* (7), 489-493. DOI: 10.1080/10601325.2017.1320754.
6. Coombs Obrien, J.; Torrente-Murciano, L.; Mattia, D.; Scott, J. L., Continuous Production of Cellulose Microbeads via Membrane Emulsification. *ACS Sust Chem Eng* **2017,** *5* (7), 5931-5939. DOI: 10.1021/acssuschemeng.7b00662.
7. Akolade, J. O.; Balogun, M.; Swanepoel, A.; Ibrahim, R. B.; Yusuf, A. A.; Labuschagne, P., Microencapsulation of eucalyptol in polyethylene glycol and polycaprolactone

using particles from gas-saturated solutions. *RSC Advances* **2019,** *9* (58), 34039-34049. DOI: 10.1039/C9RA06419B.
8. Teeka, P.; Chaiyasat, A.; Chaiyasat, P., Preparation of Poly (methyl methacrylate) Microcapsule with Encapsulated Jasmine Oil. *Energy Procedia* **2014,** *56*, 181–186. DOI: 10.1016/j.egypro.2014.07.147.
9. Microplastics. https://echa.europa.eu/hot-topics/microplastics (accessed 3 April).
10. Schwabl, P.; Köppel, S.; Königshofer, P.; Bucsics, T.; Trauner, M.; Reiberger, T.; Liebmann, B., Detection of Various Microplastics in Human Stool. *Annals of Internal Medicine* **2019,** *171* (7), 453-457. DOI: 10.7326/M19-0618.
11. Assadpour, E.; Jafari, S. M., 1 - An overview of biopolymer nanostructures for encapsulation of food ingredients. In *Biopolymer Nanostructures for Food Encapsulation Purposes*, Jafari, S. M., Ed. Academic Press: 2019; pp 1-35. DOI: https://doi.org/10.1016/B978-0-12-815663-6.00001-X.
12. Jones, O. G.; McClements, D. J., Functional Biopolymer Particles: Design, Fabrication, and Applications. *Comprehensive Reviews in Food Science and Food Safety* **2010,** *9* (4), 374-397. DOI: 10.1111/j.1541-4337.2010.00118.x.
13. Aziz, F.; Jai, J.; Raslan, R.; Subuki, I., Microencapsulation of citronella oil by complex coacervation using chitosan-gelatin (b) system: operating design, preparation and characterization. *MATEC Web of Conferences* **2016,** *69*, 04002. DOI: 10.1051/matecconf/20166904002.
14. Reddy, N., *Keratin-based Biomaterials and Bioproducts*. Smithers Rapra: 2017.
15. Holkar, C. R.; Jain, S. S.; Jadhav, A. J.; Pinjari, D. V., Valorization of keratin based waste. *Process Safety and Environmental Protection* **2018,** *115*, 85-98. DOI: https://doi.org/10.1016/j.psep.2017.08.045.
16. Yang, X.; Zhang, H.; Yuan, X.; Cui, S., Wool keratin: A novel building block for layer-by-layer self-assembly. *Journal of Colloid and Interface Science* **2009,** *336* (2), 756-760. DOI: https://doi.org/10.1016/j.jcis.2009.04.050.
17. Rajabinejad, H.; Patrucco, A.; Caringella, R.; Montarsolo, A.; Zoccola, M.; Pozzo, P. D., Preparation of keratin-based microcapsules for encapsulation of hydrophilic molecules. *Ultrasonics Sonochemistry* **2018,** *40*, 527-532. DOI: https://doi.org/10.1016/j.ultsonch.2017.07.039.
18. Islam, S.; Bhuiyan, M. A. R.; Islam, M. N., Chitin and Chitosan: Structure, Properties and Applications in Biomedical Engineering. *Journal of Polymers and the Environment* **2017,** *25* (3), 854-866. DOI: 10.1007/s10924-016-0865-5.
19. Yan, N.; Chen, X., Sustainability: Don't waste seafood waste. *Nature* **2015,** *524*, 155-7. DOI: 10.1038/524155a.
20. Mohammed, M. A.; Syeda, J. T. M.; Wasan, K. M.; Wasan, E. K., An Overview of Chitosan Nanoparticles and Its Application in Non-Parenteral Drug Delivery. *Pharmaceutics* **2017,** *9* (4), 53. DOI: 10.3390/pharmaceutics9040053.
21. Tanabe, T.; Okitsu, N.; Tachibana, A.; Yamauchi, K., Preparation and characterization of keratin–chitosan composite film. *Biomaterials* **2002,** *23* (3), 817-825. DOI: https://doi.org/10.1016/S0142-9612(01)00187-9.
22. Butstraen, C.; Salaün, F., Preparation of microcapsules by complex coacervation of gum Arabic and chitosan. *Carbohydrate Polymers* **2014,** *99*, 608-616. DOI: https://doi.org/10.1016/j.carbpol.2013.09.006.

23. Huang, H.; Yuan, W.-K.; Chen, X., Microencapsulation Based on Emulsification for Producing Pharmaceutical Products: A Literature Review. *Developments in Chemical Engineering and Mineral Processing* **2008,** *14*, 515-544. DOI: 10.1002/apj.5500140318.
24. Bah, M. G.; Bilal, H. M.; Wang, J., Fabrication and application of complex microcapsules: a review. *Soft Matter* **2020,** *16* (3), 570-590. DOI: 10.1039/C9SM01634A.
25. Manga, M.; Cayre, O.; Williams, R.; Biggs, S.; York, D., Production of solid-stabilised emulsions through rotational membrane emulsification: Influence of particle adsorption kinetics. *Soft Matter* **2012,** *8*, 1532-1538. DOI: 10.1039/C1SM06547E.
26. Pedro, S. S.; Serena, M.; Marijana, M. D.; Victor, M. S.; Richard, G. H., Water in oil emulsions from hydrophobized metal membranes and characterization of dynamic interfacial tension in membrane emulsification. *Colloids and Surfaces A: Physicochemical and Engineering Aspects* **2017,** *532*, 77-86. DOI: https://doi.org/10.1016/j.colsurfa.2017.06.051.
27. Ge, Y.; Zhang, Y.; He, S.; Nie, F.; Teng, G.; Gu, N., Fluorescence Modified Chitosan-Coated Magnetic Nanoparticles for High-Efficient Cellular Imaging. *Nanoscale Research Letters* **2009,** *4* (4), 287. DOI: 10.1007/s11671-008-9239-9.
28. McKittrick, J.; Chen, P. Y.; Bodde, S. G.; Yang, W.; Novitskaya, E., The Structure, Functions, and Mechanical Properties of Keratin. *JOM: the journal of the Minerals, Metals & Materials Society* **2012,** *64*, 449-468. DOI: 10.1007/s11837-012-0302-8.
29. Schrooyen, P. M. M.; Dijkstra, P. J.; Oberthür, R. C.; Bantjes, A.; Feijen, J., Stabilization of Solutions of Feather Keratins by Sodium Dodecyl Sulfate. *Journal of Colloid and Interface Science* **2001,** *240* (1), 30-39. DOI: https://doi.org/10.1006/jcis.2001.7673.
30. Ramanery, F.; Mansur, A.; Mansur, H., One-step colloidal synthesis of biocompatible water-soluble ZnS quantum dot/chitosan nanoconjugates. *Nanoscale research letters* **2013,** *8*, 512. DOI: 10.1186/1556-276X-8-512.
31. Ward, W. H.; Binkley, C. H.; Snell, N. S., Amino Acid Composition of Normal Wools, Wool Fractions, Mohair, Feather, and Feather Fractions. *Textile research journal.* **1955,** *25* (4), 314-325.
32. Rinaudo, M., Chitin and chitosan: Properties and applications. *Progress in Polymer Science* **2006,** *31* (7), 603-632. DOI: https://doi.org/10.1016/j.progpolymsci.2006.06.001.
33. Williams, R. A.; Peng, S. J.; Wheeler, D. A.; Morley, N. C.; Taylor, D.; Whalley, M.; Houldsworth, D. W., Controlled Production of Emulsions Using a Crossflow Membrane: Part II: Industrial Scale Manufacture. *Chemical Engineering Research and Design* **1998,** *76* (8), 902-910. DOI: 10.1205/026387698525702.
34. Stillwell, M. T.; Holdich, R. G.; Kosvintsev, S. R.; Gasparini, G.; Cumming, I. W., Stirred Cell Membrane Emulsification and Factors Influencing Dispersion Drop Size and Uniformity. *Ind Eng Chem Res* **2007,** *46* (3), 965-972. DOI: 10.1021/ie0611094.
35. Bertrandias, A.; Duval, H.; Casalinho, J.; Giorgi, M.-L., Dripping to jetting transition for cross-flowing liquids. *Physics of Fluids* **2017,** *29*, 044102. DOI: 10.1063/1.4979266.
36. Perrier, E.; Hart, J., 37 - Smart Vectorization: Enzymatically Activated Encapsulation Technologies. In *Delivery System Handbook for Personal Care and Cosmetic Products*, Rosen, M. R., Ed. William Andrew Publishing: Norwich, NY, 2005; pp 797-816. DOI: https://doi.org/10.1016/B978-081551504-3.50042-0.
37. Yuan, Y.; Kong, Z.-Y.; Sun, Y.-E.; Zeng, Q.-Z.; Yang, X.-Q., Complex coacervation of soy protein with chitosan: Constructing antioxidant microcapsule for algal oil delivery. *LWT* **2017,** *75*, 171-179. DOI: https://doi.org/10.1016/j.lwt.2016.08.045.

38. Maitra, J.; Shukla, V. K., Cross-linking in hydrogels-a review. *Am. J. Polym. Sci* **2014,** *4* (2), 25-31. DOI: 10.5923/j.ajps.20140402.01.
39. Du, J. R.; Hsu, L. H.; Xiao, E. S.; Guo, X.; Zhang, Y.; Feng, X., Using genipin as a "green" crosslinker to fabricate chitosan membranes for pervaporative dehydration of isopropanol. *Separation and Purification Technology* **2020,** *244*. DOI: 10.1016/j.seppur.2020.116843.
40. Holdich, R.; Dragosavac, M.; Williams, B.; Trotter, S., High throughput membrane emulsification using a single-pass annular flow crossflow membrane. *AIChE Journal* **2020**, e16958. DOI: 10.1002/aic.16958.
41. Albisa, A.; Piacentini, E.; Arruebo, M.; Sebastian, V.; Giorno, L., Sustainable Production of Drug-Loaded Particles by Membrane Emulsification. *ACS Sustainable Chemistry & Engineering* **2018,** *6* (5), 6663-6674. DOI: 10.1021/acssuschemeng.8b00401 .

SYNOPSIS

Microcapsules of sunflower oil in sustainable biomaterials were made by low-energy membrane emulsification with keratin and interfacial deposition of oppositely charged chitosan.

For Table of Contents Use Only